Optica Applicata, Vol. XIX, No. 4, 1989

Diffraction-pattern sampling and its applications in optical metrology

C. GORECKI

Laboratoire d'Optique P. M. Duffieux (URA CNRS no. 214), Université de Franche-Comté, Route de Gray, 25030 Besançon Cédex, France.

This paper describes two industrial applications of diffraction-pattern sampling in optical metrology: it covers rough surface classification and particle size analysis. The both setups consist of a coherent optical system to generate the Fourier irradiance of a sample and a digital computer to process data. The sampling of optical power spectrum is achieved with a wedge ring detector. The experimental results show the potentials of these techniques for performing various aspects of automatic industrial inspection system.

1. Introduction

The diffraction techniques of an object contains a distribution of the spatial frequencies present in the input object. It provides direct information about the textural properties of images as well as other image characteristics.

Fourier techniques has been proved useful in optical processing for a wide variety of applications including automatic pattern recognition [1], [2], quality control problems [3] or particle analysis devices [4]. An interesting Fourier spectrum sampler developed originally by KASDEN [5] is wedge ring detector. It forms a polar sampling geometry and allows flexible and dimensionally reduced measurement basis in Fourier space.

In this paper, two different systems for automatic wedge ring sampling of Fourier spectra are proposed. The first method is a machined metal surface classification device [6]. The second method is an optical particle size analyzer [7]. In each case the experimental results demonstrate the utility of optical power spectrum sampling for automatic pattern classification.

2. Diffraction-pattern analysis

The automatic optical spectrum analyzer includes a Fourier transforming lens, a detector, and an electronic system interfaced to a microcomputer. A detector made by Recognition Systems was used to sample the light intensity distribution in the diffraction pattern plane of an input sample. The detector consisted of 32 wedge sections and 32 ring elements (Fig. 1). The all 64 outputs were amplified by analog circuitry (Fig. 2). Each signal is connected to an individual preamplifier and a sample-and-hold amplifier which was multiplexed into an autoranging amplifier and A/D converter. An IBM–AT computer is used for digital processing.

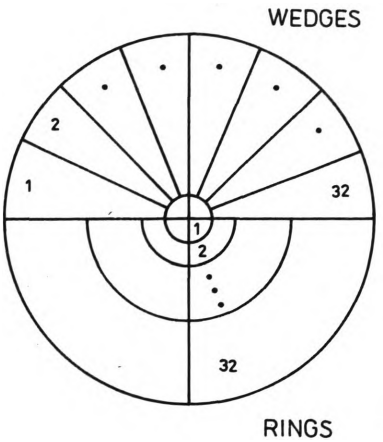

Fig. 1. Wedge ring detector geometry

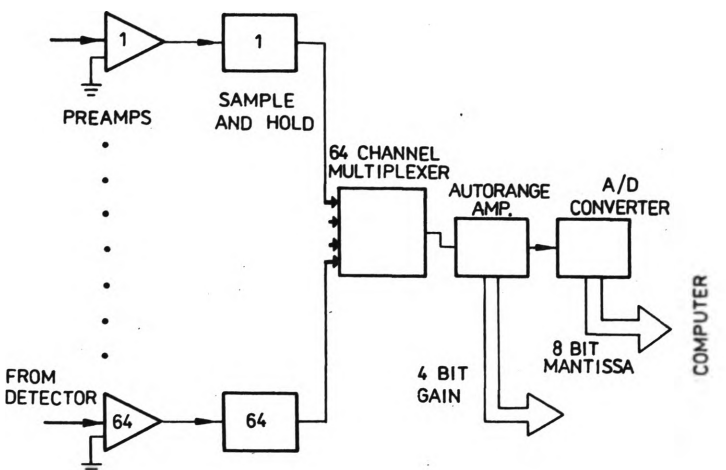

Fig. 2. Block diagram of the electronic system

Let $g(x, y)$ be the field distribution in the input sample plane; then the Fourier transform of $g(x, y)$ is

$$G(u, v) = \frac{k}{\lambda f} \iint_{-\infty}^{+\infty} g(x, y) e^{-j2\pi/\lambda f [ux + vy]} dxdy \tag{1}$$

where k is the amplitude of the incident monochromatic wave, λ is the laser wavelength, and f is the focal length of the Fourier transforming lens. Here $u = x/\lambda f$ and $v = y/\lambda f$ are spatial frequency coordinates in the Fourier space.

The j-th ring output is

$$r_j = \int_0^{2\pi} \int_{\varrho_j}^{\varrho_j + \Delta\varrho_j} |G(\varrho, \Phi)|^2 \varrho d\varrho d\Phi, \quad j = 1, \ldots, 32 \tag{2}$$

where $\varrho = (u^2 + v^2)^{1/2}$ and $\Phi = \tan^{-1}(v/u)$ and r_j represents the total power carried by a ring with inner radius ϱ_j and outher radius $\varrho_j + \Delta\varrho_j$.

The j-th wedge output is

$$w_j = \int_0^{\varrho_{max}} \int_{\Phi_j}^{\Phi_j + \Delta\Phi} |G(\varrho, \Phi)|^2 \varrho d\varrho d\Phi, \quad j = 1, \ldots, 32. \tag{3}$$

w_j represents the total power in the range of directions defined by the $(\Phi_j, \Phi_j + \Delta\Phi)$ coordinates and the spatial frequencies within the range $(0, \varrho_{max})$. The wedge ring detector sampling is very attractive because the ring outputs are invariant to rotation and wedge outputs are invariant to scale changes in the sample plane.

Once digitized, Fourier spectrum data are stored in a 64 component vector. All data are normalized to the laser power to minimize noise due to variation in laser power level and detector electronic noise. The discrete form of the ring elements helps to smooth the Fourier spectrum and reduces the speckle. The suitable spatial frequency sampling range is limited by the diffraction zero-order and the highest sampled spatial frequency determined by the electronic noise in the system. The determination of this effective sampling range is a part of the calibration procedure.

Also, the spectrum measurements generate a statistical stable recorded diffraction pattern.

3. Roughness classification system

Various optical methods have been proposed for measuring the roughness of nonoptical surfaces [8]–[10]. The present work deals with the direct wedge ring sampling of the optical spectra from flat machined samples. Analysis of such spectra will provide a practical tool for the assessment of the surface classification [11].

3.1. Experimental setup

The optical system is shown in Fig. 3. The rough sample is illuminated by a monochromatic convergent beam. A transform lens L_2 generates the Fourier transform of the input data. The lateral resolution of the optical system is about 10 μm.

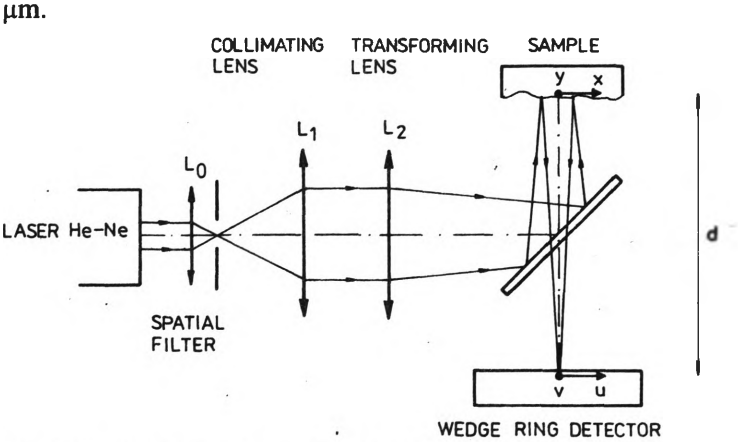

Fig. 3. Optical system for surface classification

3.2. Classification algorithm

The wedge ring detector sampling is used as a preprocessor which reduces an infinitely dimensioned spectrum image into a set of 64 measurements. The role of digital processing then is to implement and automatic procedure which can assign the appropriate class label to a test rough sample represented by a 64-component vector. Given this sample vector, a feature selection procedure is required to further reduce dimensionality which helps to minimize training set size, computer storage and processing time. A classification procedure is then required for partition of the feature space into regions corresponding to different classes. Thus, by detecting the separation between the samples in feature-space, surface classification can be achieved.

Statistical global features having good radial and angular discriminatory properties are defined as follows:

i) Total energy

$$E_t = \sum_{i=1}^{32} r_i \tag{4}$$

where r_i represents the i-th ring reading.

ii) Radial normalized slope to spatial frequency v_i

$$\gamma_i = v_{i+1} R_{i+1} - v_{i-1} R_{i-1} \tag{5}$$

where R_i is the i-th normalized ring reading.

iii) Radial normalized variance.

$$\sigma_R^2 = \frac{1}{N-1} \sum_{i=1}^{N} \left[\beta_i R_i - \left[\frac{1}{N} \sum_{i=1}^{N} \beta_i R_i \right]^2 \right]^2 \tag{6}$$

where $\beta_i = v_i/(v_{i=1} - v_i)$ and $1 < N < 32$.

iv) Maximum radial difference

$$D_{\max} = \max \left[\frac{|R_i - \mathscr{R}_i|}{R_i} \right] \tag{7}$$

where $\mathscr{R}_i$ represents a ring element of normalized reference sample vector.

v) Radial correlation coefficient

$$\varrho_R^k = \frac{32 \sum_{i=1}^{32} R_i \mathscr{R}_i^k - \sum_{i=1}^{32} R_i \sum_{i=1}^{32} \mathscr{R}_i^k}{(\sigma_R \sigma_R^k)^{1/2}} \tag{8}$$

where k denotes the sample class number, $\mathscr{R}_i^k$ represents the ring model vector components and σ_R^k is the standard deviation of class k.

vi) Angular mean value

$$\langle W \rangle = \frac{1}{32} \sum_{i=1}^{32} W_i \tag{9}$$

where W_i is the normalized wedge reading.

vii) Angular variance

$$\sigma_W^2 = \frac{1}{32} \sum_{i=1}^{32} (W_i - \langle W \rangle)^2. \tag{10}$$

viii) Angular range

$$\Delta W = W_{max} - W_{min} \tag{11}$$

where W_{max} and W_{min} represent the extremum wedge values.

ix) Angular correlation coefficient

$$\varrho_W^k = \frac{32 \sum_{i=1}^{32} W_i \mathscr{W}_i^k - \sum_{i=1}^{32} W_i \sum_{i=1}^{32} \mathscr{W}_i^k}{(\varrho_W \varrho_W^k)^{1/2}} \tag{12}$$

where $\mathscr{W}_i^k$ represents the wedge model vector elements, and σ_W^k is the standard deviation of class k.

The selected features are used as parameters of the discriminant functions for the classification procedure. The classification algorithm provides automatically the linear combination of the features adapted to the solution of our specific classification problem.

Let N_T be the total number of rough samples. The first step of the classification procedure is based on an optimal selection of roughness features. We select, among the p potential features, the $s (s \leqslant p)$ ones such that the set of discriminant functions involving these features leads to the optimal classification of the N_T samples. In the p-dimensional feature space, we can use the interclass distance measurement between j and j' classes as the feature selection criterion [12]

$$d = \sum_{k=1}^{s} [A_{jk} - A_{j'k}][\mu_{jk} - \mu_{j'k}] \tag{13}$$

where j and $j' = 1, \ldots, q$, q is the number of different classes, and μ_{jk} represents the mean value of feature k for class j.

The A_{jk} and $A_{j'k}$ coefficients are determined using N_T rough samples of the training set. The distance d describes the classification performance; we use the minimization of the distance d as the decision rule

$$\delta = \min_i d \text{ assign class label } i. \tag{14}$$

3.3. Results

As a specific example of application to classification consider the photomicrographs of two flat steel samples and the associated optical power spectra illustrated in Fig. 4. The surface of the first sample has undergone laser treatment. The second samples has a surface produced by grinding. Fig. 5 shows, respectively, the ring irradiance distributions with the corresponding frequency sampling range for both classes. A wedge intensity distribution for the two test samples is given in Fig. 6.

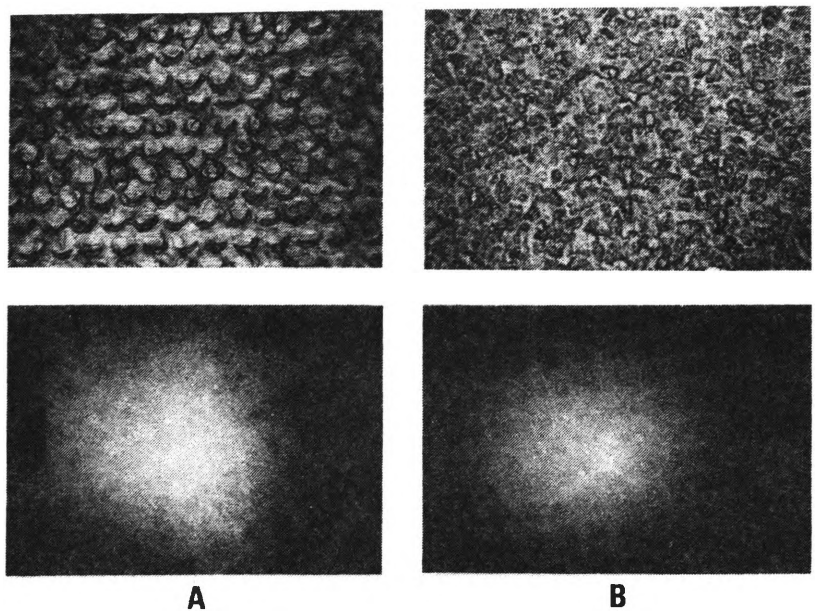

Fig. 4. Photomicrographs (× 50) and the associated Fourier spectra of the laser treated (A) and ground (B) samples

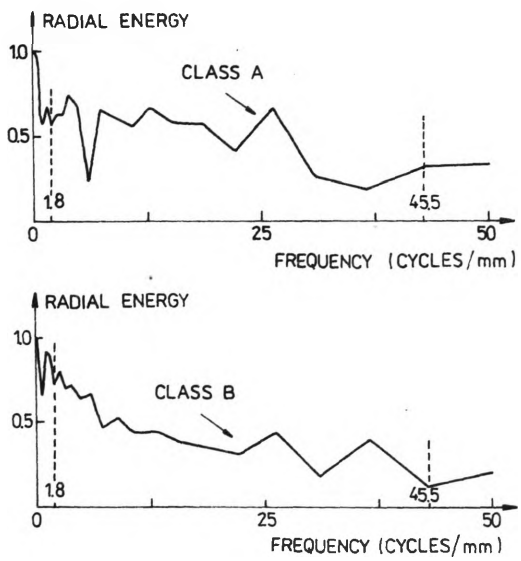

Fig. 5. Ring intensity distributions of the laser treated and ground samples (for A and B see Fig. 4)

To classify 70 rough samples divided into two classes, the algorithm has selected seven features which are represented in the Table. Figure 7 shows the variation of the classification error as a function of the number of features used in the discrimination procedure: the error value decreases as a function of the selected features. The use of two of these features to provide separation between laser treatment and ground data is shown in Fig. 8: it appears that the radial and angular variances can be used to achieve roughness classification. The classification error is about 15%. When a 7-D feature space is used, the classification error is about 6%.

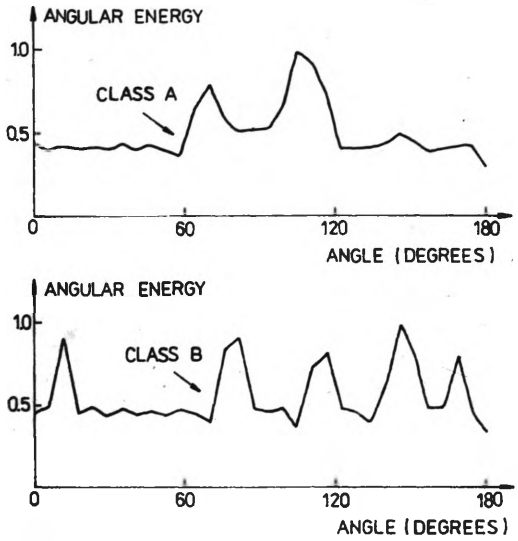

Fig. 6. Wedge intensity distributions of the laser treated and ground samples (for A and B see Fig. 4)

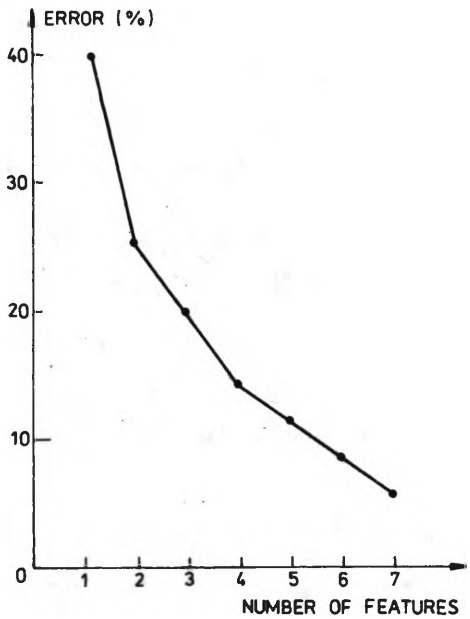

Fig. 7. Percentage of classification error with the number of selection rules

Seven feature-spaces selectioned for laser and ground samples

Feature-spaces Features selectioned	Number of features	Classification error number (total number: 35)	Percentage of correct
Angular variance	1	14	60
Radial variance	2	9	74.3
Total energy	3	7	80
Angular range	4	5	85.7
Radial slope	5	4	81.6
Radial correlation	6	3	91.4
Maximum of the radial difference	7	2	94.3

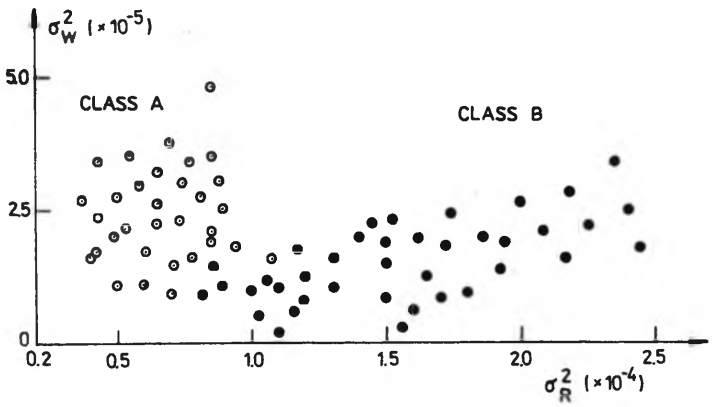

Fig. 8. Example of 2-D feature-space

4. Optical analyzer of PbS substrate

Many industrial powders are quasicircular, and their diffraction pattern have rotational symmetry. To automatically classify such grain populations, we present a Fourier spectrum analyzer that uses wedge ring detector sampling. A procedure based on least-squares inversion of measurements is implemented to estimate particle-size distribution [7].

4.1. Basic concept

In polar coordinates the amplitude transmittance of a quasicircular particle can be analysed into circular harmonics

$$g(r, \theta) = \sum_{k=-\infty}^{\infty} g_k(r)\, e^{jk\theta} \tag{15}$$

where g_k is the Fourier coefficient of the k-th order. The Fourier transform of $g(r, \theta)$ is

$$G(\varrho, \theta) = \sum_{k=-\infty}^{\infty} G_k(\varrho)\, e^{jk(\theta - \pi/2)}. \tag{16}$$

This result can be extended to a random population of grains with varying mean diameter divided into c granulometric classes. Let N_j be the population of class j. The total particle number is given by

$$N_0 = \sum_{j=1}^{\infty} N_j. \tag{17}$$

The total intensity in the transform plane is then a superimposition of c Airy's patterns [13]

$$|G_N(\varrho, \theta)|^2 = \sum_{j=1}^{c} N_j \sum_{k=-\infty} |G_{jk}(\varrho)|^2. \tag{18}$$

All diffraction patterns produce a symmetric spectrum. Since the components obtained from ring integrations give, all information about the rotationally symmetric portion of the spectrum, our sampling base data will consist of radial samples. The Fourier irradiance at discrete spatial frequencies ϱ_i can be written

$$I_N(\varrho_i) = \sum_{j=1}^{c} N_j S_{ij} + n(\varrho_i) \tag{19}$$

with $S_{ij} = \sum_{k=-\infty}^{\infty} |G_{ik}(\varrho_i)|^2$ and $i = 1, \ldots, 32$.

Let $\boldsymbol{N}$ be the class population vector, $\boldsymbol{N} = (N_1, \ldots, N_c)^{\mathrm{T}}$. The irradiance data vector can be written in matrix notation [7]

$$\boldsymbol{I}' = \boldsymbol{K}(\boldsymbol{I}\boldsymbol{N} + \boldsymbol{n}) = \boldsymbol{K}\boldsymbol{S}\boldsymbol{N} + \boldsymbol{n}' \tag{20}$$

where $\boldsymbol{S}$ denotes the matrix (S_{ij}) with components defined below, $\boldsymbol{n}'$ is the noise data vector and $\boldsymbol{K}$ represents the photometric calibration matrix.

Estimation of the vector $\boldsymbol{N}$ is obtained by implementing a minimum mean-square error criterion, which can be written [14]

$$\mathfrak{N} = [(\boldsymbol{W}\boldsymbol{K}\boldsymbol{S})^{\mathrm{T}} (\boldsymbol{W}\boldsymbol{K}\boldsymbol{S})]^{-1} (\boldsymbol{W}\boldsymbol{K}\boldsymbol{S})^{\mathrm{T}} \boldsymbol{W}\boldsymbol{I}'. \tag{21}$$

Matrix elements S_{ij} can be calculated analytically by using the Fraunhofer theory. For a particle of radius a_j the normalized energy carried by a ring with inner radius ϱ_i and outer radius ϱ_{i+1} is

$$S_{ij} = \alpha \pi a_j^2 (\gamma a_j/2)^2 [\varrho_{i+1}^2 - \varrho_i^2] \tag{22}$$

where $\gamma = 2\pi/\lambda f$, $i = 1, \ldots, 32$, $j = 1, \ldots, c$ and α represents a parameter of the optical system.

4.2. Experimental setup

Figure 9 shows the optical system where the coherent beam is spatially filtered, then expanded and collimated. A transform lens L_2 generates the Fourier spectrum of the

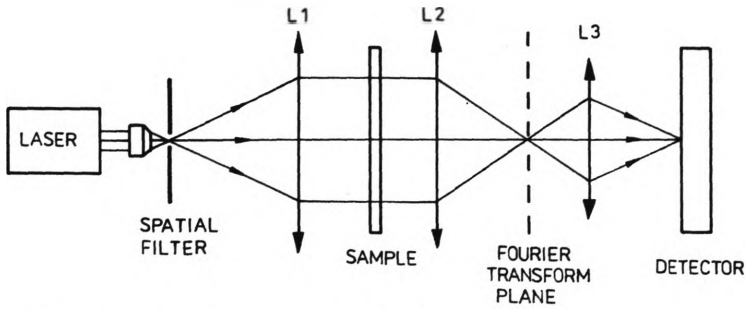

Fig. 9. Optical system for particle analysis

diffracting sample, and a lens L_3 projects an englarged image of Fourier spectra onto wedge ring detector. The configuration of optical system was such that all frequencies were sampled up to 50 cycles/mm.

4.3. Results

The results of particle-size estimation are described with a specific application in granulometric analysis of PbS substrate. Fig. 10 shows a portion of this sample. Grain sizes are divided in eight different classes in the range of 25 to 320 μm. To prevent the superimposition of any particles, a glass plate is used on which particles are deposited in thin layer. This sample is coated with a transparent film.

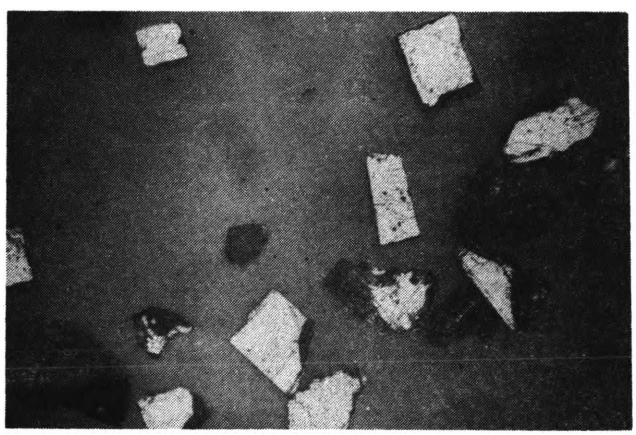

Fig. 10. Photomicrograph (× 100) of the PbS sample

For each of the eight granulometric classes we consider the Rayleigh curve (Fig. 11), which gives the normalized fraction of the total energy in a diffraction pattern that falls within a circle of radius ϱ_i corresponding to the spatial frequency v_i. If we wish to calculate the matrix components S_{ij} of the j-th ring, we determine the

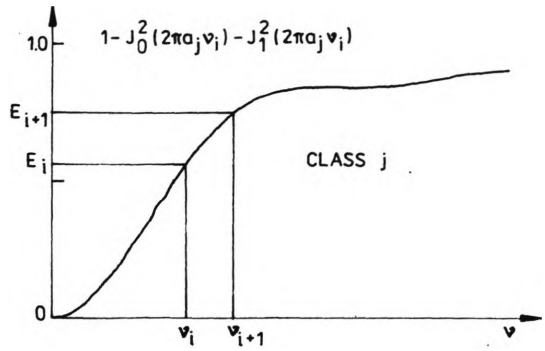

Fig. 11. Plot of the Raileigh curve for a_j particle diameter

curve area limited by the ring sampling frequency ν_i and ν_{i+1}. Figure 12 shows for a PbS sample a smoothed Fourier spectrum with the corresponding frequency range. The limits of the frequency sampling range are determined by central mask and the noise level. The histogram of PbS particle-size distribution is shown in Fig. 13. The estimation error increases as the particle diameter decreases, as shown in Fig. 14 for each class diameter.

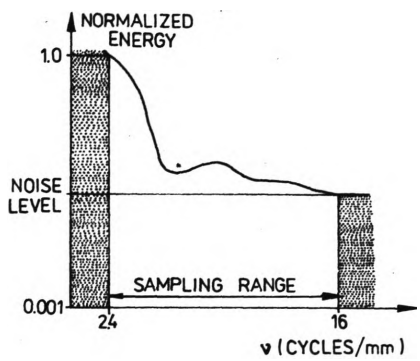

Fig. 12. Plot of the normalized radial energy distribution (log scale) in the smoothed spectrum of the PbS sample

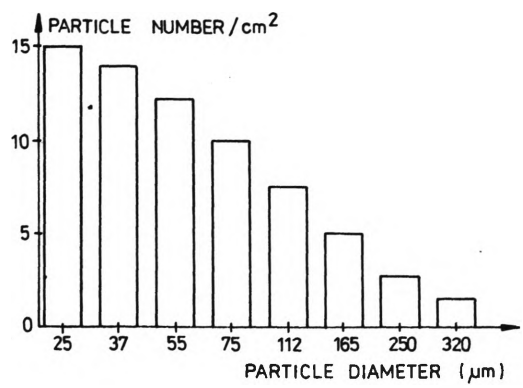

Fig. 13. Histogram of PbS particle-size distribution

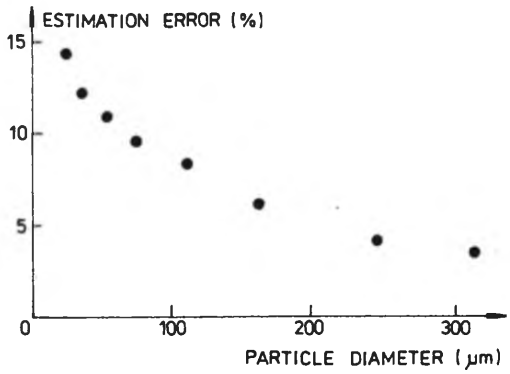

Fig. 14. Estimation error for each class diameter

5. Conclusions

Two optical/digital methods has been studied using an optical transform system with a wedge ring detector for Fourier spectra sampling. The technique provides an interesting combination of the speed of optical Fourier analysis with the flexibility of digital processing. The simplicity of the procedure based on radial and angular sampling of the diffraction pattern associated with the classification or estimation methods, allows a statistical and quantitative analysis of the data set. Relatively simple feature selection algorithms reduce the dimensionality of sampled data. Hardware interfaced to a small computer is available at modest cost.

References

[1] LENDARIS G. G., STANLEY G. L., Proc. IEEE **58** (1970), 198.
[2] LUKES G. E., Proc. SPIE **45** (1974), 265.
[3] KASDAN H. L., MEAD D. C., *Proc. Electroopt. System Design*, Aneheim–CA, 1975, 248.
[4] CORNILLAUT J., Appl. Opt. **11** (1972), 265.
[5] KASDAN H. L., Proc. SPIE **117** (1977), 67.
[6] GORECKI C., Proc. SPIE **954** (1988), 272.
[7] GORECKI C., Opt. Eng. **27** (1988), 466.
[8] FUJI H., ASAKURA T., J. Opt. Soc. Am. **67** (1977), 1171.
[9] ALLARDYCE K. K., GEORGE N., Appl. Opt. **26** (1987), 2364.
[10] BHUSHAN B., WYANT J. C., KOLIOPOULOS L., Appl. Opt. **24** (1985), 1489.
[11] GORECKI C., Opt. Laser Technol. **21** (1989), 117.
[12] HE D.-C., WANG L., GUIBERT J., Patt. Recognition **21** (1988), 141.
[13] ANDERSON W. L., BEISSNER R. E., Appl. Opt. **10** (1971), 1503.
[14] STARK H., LEE D., KOO B. W., Appl. Opt. **15** (1976), 2246.

Received July 24, 1989

Стробирование дифракционного спектра и его применение в метрологии

Описаны два применения в промышленной метрологии стробирования дифракционного спектра. Они касаются классификации шероховатых поверхностей и анализа размеров частиц. Два

измерительных места заключают в себе конкретную оптическую систему генерирующую спектр Фурье пробки и компьютер для обработки данных. Оптическое стробирование спектра мощности происходит с помощью кольцевого детектора. Итоги экспериментальных исследований показывают возможности этих техник в пределах разных аспектов автоматических промышленных контрольных систем.